

**PRE-PROOF FILE**

# Synthesis of Hydroxyapatite from Budu Waste by Calcination Method

**Daupor, Hasan**<sup>\*+</sup>*Chemistry Program, Faculty of Science Technology and Agriculture, Yala Rajabhat University, Yala, THAILAND***Wijaya, Anugrah Ricky***Chemistry Department, Faculty of Mathematics and Natural Science, Universitas Negeri Malang (UM), Malang, INDONESIA***Amornpitoksuk, Pongsaton***Division of Physical Science, Faculty of Science, Prince of Songkla University, Hat Yai, Songkhla, THAILAND***Chelong, Isma-ae***Biology Program, Faculty of Science Technology and Agriculture, Yala Rajabhat University, Yala, THAILAND***Suksuwan, Acharee***The Halal Science Center, Chulalongkorn University, Bangkok, THAILAND*

**ABSTRACT:** Fish bones contain high calcium, which makes them a good raw material for the preparation of calcium hydroxyapatite (HAp). HAp is usually prepared from fresh fish bones because it has low impurity but there are many waste fish bones from food processing. In this work, HAp was synthesized from Budu waste by maceration process and calcination. Obtained products were characterized by X-ray diffraction (XRD), Fourier transform spectroscopy (FT-IR), and thermal analysis. When the calcination was higher than 600 °C, the product showed a mixture of hydroxyapatite  $[Ca_5(PO_4)_3OH]$  as a major phase and merrillite  $[Ca_9MgNa(PO_4)_7]$  as a minor phase. The amount of merrillite was increased with an increase in calcination temperature.

**KEYWORDS:** Fish bone waste; Hydroxyapatite; Merrillite mineral; Calcination method; Phase transformation.

## INTRODUCTION

Budu or southern Thailand style-fish sauce is a favourite side dish in the Southern Border Provinces, especially in the Sai Buri district of Pattani Province. It is usually served with mixed vegetables and peppers or

kneaded into cooked rice. Budu is a One Tambon One Product (OTOP) sold by two brands - Budu Heng and Budu Yiseng, produced by the digestion of enzymes and microorganisms from small fishes such as *Stolephorus*

---

\* To whom correspondence should be addressed.

+ E-mail: hasan.d@yru.ac.th

1021-9986/2022/12/4127-4136

10/\$/6.00

*indicus*, *Clupeoides sp.*, *Sardine sp.*, *Pinalopingalo*, or *Decapterusrusselli*. The process starts by fermenting the fish with its tripe intact using sea salt at a fish-to-salt ratio of 3:1 for 8-12 months shorter than is than usual of fish source fermented at around 18 months, then transfers to the heating process. The fermented fish and bones produce a black liquid called Budu mixed with residues of precipitated and dispersed fish bones, fins, and fish meat. These residues, considered as wastes in Budu production, are great sources of calcium, phosphorus, proteins, and nutrients.

The calcium phosphates present in Budu waste are well known for their use as biomaterials [1]. Among these phosphates, hydroxyapatite (HAp) is probably the most important one owing to its very high biocompatibility, bioactivity, and osteoconductivity, as well as its anti-inflammatory and anti-immunogenicity properties. Based on the structure and chemical properties, HAp with a molar ratio of  $\text{Ca/P} = 1.67$  is common in inorganic compounds found in bones and teeth. Therefore, this compound is used for various biomedical applications such as orthopedic and dental implants [1, 2], fillers for dental adhesives, drug delivery agents, and biosensor applications [3]. The extraction of HAp from solid fish canning residues both scales and bones under thermally treated at 1300 °C has been reported [4]. The HAp growth initiates as proteins and other nutrients from the residues decompose when calcined at high temperatures up to 900 °C [5].

HAp has been synthesized from various sources of animal bones [6]. In synthesising HAp from tuna bones (*Thunnus obesus*), the process starts with washing the bones with hot tap water to remove remaining fish meat, followed by washing with NaOH and acetone to remove dirt, proteins, fats, and other organic substances. The collagen is then hydrolysed with 2 M NaOH for 5 hours at 250 °C and finally burned at 900 °C for 5 hours to completely remove the organic matter from the bone and extract HAp [4]. Recently, HAp synthesis using a subcritical water process and alkaline hydrothermal hydrolysis of different fish bones such as those from Japanese sea bream [7], Brazilian river fish [8], and Atlantic swordfish [9] was reported. These processes utilize thermal treatment methods for successful HAp extraction. Other methods of extracting HAp include microwave-assisted, hydrothermal, and ultrasonic irradiation processes [10-12]. Furthermore, HAp exhibits

various morphologies, out of which spherical-like HAp particles were prepared by the co-precipitation method in Simulated Body Fluids (SBF) solutions [13]. Novel catalyst the  $\gamma\text{-Fe}_2\text{O}_3\text{@HAp@}\beta\text{-CD}$  core-shell nanoparticles were utilized to prepare a  $\beta$ -azidoalcohols,  $\beta$ -nitroalcohols, and  $\beta$ -cyanohydrins [14]. However, these methods are long and expensive. By far, only the calcination method, which is simpler and requires less energy compared to the other methods, successfully obtains HAp with high biocompatibility. Thus, there is a need to develop a simpler and more cost-efficient HAp synthesis process. Table 1 summarises the properties of HAp synthesized from various fish bones. In short, the calcination of fish bone at increasing temperatures will appear the other calcium phosphate mixed with HAp [15-20].

This research reports a new method to synthesise HAp from the dispersed fishbone residues in Budu. The anchovy fish bones local to the three Southern Border Provinces of Thailand are collected and converted into HAp using an acid-alkaline hydrolysis method. The bones are also treated in solution prior to calcination to change their composition. This novel material and method combination offers a cheaper HAp synthesis alternative and helps reduce the environmental problems caused by waste bones in Budu manufacturing.

## EXPERIMENTAL SECTION

### Calcination method synthesis

The anchovy fish bones were collected from BuduYiseng waste and washed with water to remove the remaining traces of meat and skin. After thorough washing, the bones were dried at 60 °C and were ground using mortar and pestle. The acid-alkaline hydrolysis method was followed to hydrolyse the collagen and other organic moieties. First, 20 g of ground anchovy bone was treated with 1 M HCl continuously stirring for 12 hours (solid-liquid ratio=1:2). After that, the treated sample was stirred in 1 M NaOH for 12 hours. The mixture was filtered in a suction pump with continuous washing with water and dried in an oven at 100 °C. The Budu waste sample was obtained and referred to as BW. Then, 1 g of the dried fish bone was added in a silica crucible and was calcined at temperatures of 300 °C, 400 °C, 500 °C, 600 °C, 700 °C, and 800 °C for 3 hours in an electric muffle furnace. Lastly, the white powder of HAp was extracted as shown in Fig. 1.

Table 1: Summary of HAp properties synthesised from various fish sources

No	Fish source	Method	Temperature and time	Crystalline phase	Morphology	Ref
1	Tilapia fish	Calcination	800-1000 °C for 5 h	HAp	Sphere	[15]
2	Roho labio	Calcination	650 °C	HAp + $\beta$ -TCP	Large agglomerated	[16]
3	Bluefin trevally	Calcination	750 °C for 5 h	HAp	Irregular	[17]
4	<i>C. chanos</i> <i>T. crocodilus</i> <i>C. batrachus</i>	Calcination	1000 °C	HAp + $\beta$ -TCP	-	[18]
5	Tuna fish		700-1100 °C	HAp + $\beta$ -TCP	Sphere + irregular	[19]
6	Milkfish	Calcination	600-800 °C for 5 h	$\text{Ca}_{10}(\text{PO}_4)_6(\text{CO}_3)_2$ $\text{Ca}_{10}(\text{PO}_4)_3(\text{CO}_3)_3(\text{OH})_2$ , $\text{Ca}_3(\text{PO}_4)_2$ , $\text{Ca}_8\text{H}_2(\text{PO}_4)_6$	-	[20]

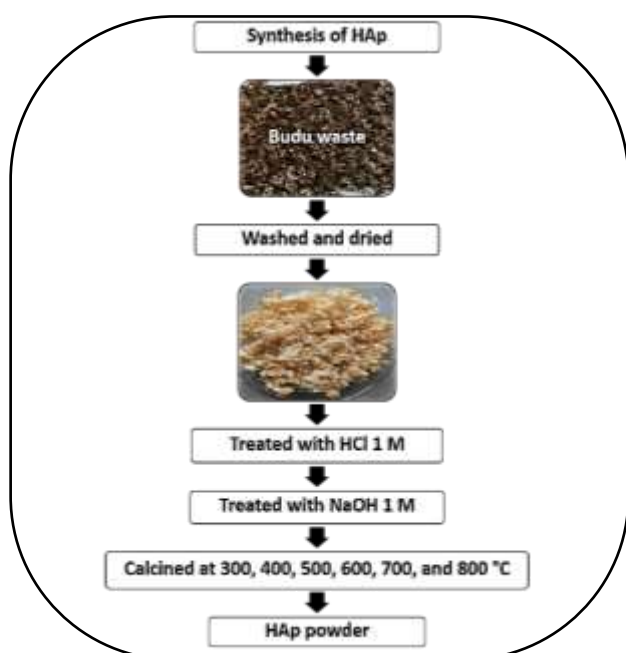


Fig. 1: Schematic representation of synthesis of HAp from Budu waste

### Phase analysis of the synthesized powder

Thermal behaviors of HAp powders were investigated by thermogravimetry/differential thermal analysis (TGA/DTA7, Perkin Elmer, USA) with heating temperature ranges from 100°C to 1000°C at a heating rate of 10°C min<sup>-1</sup>. The HAp functional groups were identified using a Fourier transform infrared spectroscopy (FT-IR, JASCO6800), over the region 350 - 4000 cm<sup>-1</sup> under KBr pellet technique. The size and morphology were examined using a scanning electron microscope with energy-dispersive X-ray spectroscopy (SEM/EDX) (Quanta 400, FEI, Czech Republic). Phase characterisation of the extracted powder was performed using an automated X-ray diffractometer (XRD) (Model D/MAX-B, Rigaku Co., Tokyo, Japan) with Cu K $\alpha$  radiation ( $\lambda=1.5418 \text{ \AA}$ ),

tube voltage of 35 kV, and tube current of 30 mA. With the XRD operated in scanning mode, XRD 2 $\theta$  scans were recorded from 20° to 45° with a 2 $\theta$  step size of 0.05° and a scanning rate of 1.5 °/min. Lattice parameters of obtained products were calculated by the following equation:

$$\frac{1}{d^2} = \frac{4(h^2 + hk + k^2)}{3a^2} + \frac{l^2}{c^2} \quad (1)$$

where  $d$  is the spacing between the planes in the set of Miller indices ( $h k l$ ).

The crystallite size of HAp was determined using the diffraction peak of the (0 0 2) plane and the Scherrer equation [21-23].

$$D = \frac{k\lambda}{\beta_{1/2} \cos \theta} \quad (2)$$

The degree of crystallinity was calculated using diffraction peaks (112) and (300) of HAp with the equation [24] given as:

$$X_c = \frac{I_{(300)} - V_{(112)/(300)}}{I_{(300)}} \quad (3)$$







where  $X_c$  is the fraction of crystalline phase,  $I_{300}$  is the intensity of (300) diffraction peak, and  $V_{112/300}$  is the intensity of the trough between (112) and (300) diffraction peaks of HAp.

## RESULTS AND DISCUSSION

### General observation

The sample colour changes upon annealing at different calcination temperatures, as listed in Table 2. Initially, the as-prepared Budu waste was light yellow. Upon calcination at temperatures of 400 °C, 500 °C, and 600 °C, the colour of the bone samples changed to black, light brown, and grey, respectively. However, when calcined at 700 °C, the samples turn white, suggesting a complete removal of organic substances. These series of colour changes are associated with the burn out process of the organic matrix

**Table 2: Effect of calcination temperature on the color, lattice constant, crystallinity, and crystallite size for bone samples from Budu waste**

Calcination (°C)	Photographs	Lattice constant (Å)		Crystallite size (nm.)	Crystallinity (%)
		$\alpha$	$c$		
300		8.5797	6.8831	12	30
400		8.5590	6.8797	12	32
500		8.6012	6.8819	10	31
600		9.4229	6.8522	35	49
700		9.4304	6.8768	41	64
800		9.4291	6.8585	41	64
Com HAp	White	9.4639	6.8801	41	54

(e.g., protein and collagen) in the Budu residue. The darker colours of bone samples calcined below 700 °C indicated an incomplete removal of organic compounds.

#### Phase transition

Fig. 2 shows the XRD patterns of raw Budu waste (BW), treated Budu waste, and commercial HAp. All the main reflections of the treated Budu waste are in agreement with

the ICDD standard of HAp. The main lattice reflections that occur at 25.9°, 28.0°, 28.9°, 31.8°, 32.9°, 34.1°, 39.8° are the (002), (102), (120), (121), (300), (202), (310) planes of Hap crystallized in hexagonal structure (ICDD Reference No. 01-084- 1998) [25, 26]. The main peak of (121) plane is a family with (211) plane which shifted to lower 2 theta due to phase composition impurities [27, 28]. The values of lattice constant, crystallite size, and degree of crystallinity

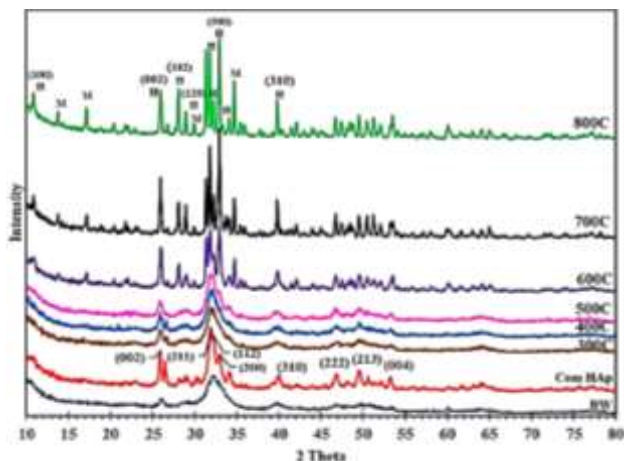


**Fig. 2:** XRD patterns for the untreated BW and calcined at different temperatures: 300, 400, 500, 600, 700 and 800 °C; (Com HAp) commercial HAp. The peaks marked with H and M represent to hydroxyapatite and merrillite mineral, respectively.

for all samples are summarized in Table 2. It observed that the lattice parameters increased with an increment of calcination temperatures due to a crystal growth at high temperature. Crystallinity of sample calcined at 800 °C was 64% that was higher than those of sample calcined at 300 °C and commercial HAp (Table 2). As shown in Fig 2, the XRD patterns of sample calcined at 300, 400, and 500 °C were identical. An additional diffraction peak at 34.6° corresponded to the merrillite phase (ICDD Reference No. 01-075- 4410) noticeably appeared in the sample calcined at 600 °C, which suggests that HAp and merrillite is the primary and secondary phase in this material, respectively. According to formation merrillite phase at high temperature, the amount of HAp was therefore decreased when the calcination temperature was risen from 600 to 800 °C. In general, the HAp can transform to whitlockite and the merrillite is usually produced by dehydrogenation of whitlockite at temperature of 1050 °C [29]. In this work, the merrillite formed at 600 °C could be attributed from a reaction between HAp and residue  $Mg^{2+}$  in the powder before calcination. Although the amount of HAp phase was reduced, the increasing calcination temperature improved the crystallinity of HAp, as evidenced by the sharper XRD peaks (Fig 2).

#### Scanning electron microscopy-energy dispersive x-ray spectroscopy results

SEM images of HAp microstructure calcined with different calcined temperatures were shown in Fig. 3. Fig.

3 a-c shows the SEM images of sample calcined at 300 °C. It observed that the sample showed an aggregation of small sphere particles on the large piece materials. The rough surface morphology was observed for sample calcined at 600 °C as shown in Fig. 3 d-e. This rough surface attributed from a formation of flower-like structure (Fig. 3f). It is observed that this unique flower-like microstructure is completely formed and assembled from microplates. The size of the flower-like HAp structure is about 30-20 μm, composed of microplates with a diameter of about 10 μm. Mapping analysis confirmed that over flower-like structure area corresponding to Mg and O elements (Fig. 4a-f). The bright green and blue over the dark (Fig. 3c and 3d) were conformed to O and Mg elements that consist in microsheets of merrillite phase forming as minor composites after calcinated at 600 °C. Therefore, the presence of Mg in the flower-like microstructure of merrillite can probably be controlled the formation of merrillite phase on the HAp surface. EDX analysis of sample with 600 °C calcination temperature (Fig. 4g) was calculated for the Ca/P ratios and found at around 2.31 which was shifted up from standard hydroxyapatite (Ca/P ratios) generally appeared at 1.67 [30]. The difference finding might be due to the fact that the implication of  $Mg^{2+}$  and  $Na^+$  in materials were 4.9% and 1.2%, respectively. The presence of merrillite phase in sample calcined at 600 °C was in agreement with the XRD results (Fig. 2).

#### Thermogravimetric analysis and differential thermal analysis

The thermal decomposition of samples with hydroxyapatite/merrillite composites was analysed through thermogravimetric and differential thermal analyses. The TGA-DTA curve recorded from the 600 °C powder sample (Fig. 5) shows a 3.01% total weight loss in the available inorganic residue, with successive losses occurring at three distinct temperature intervals. A weight loss of 0.523% was observed at temperatures between 65 °C and 200 °C, with a dip at 81 °C on the DTA plot due to a release of incorporated water molecules. In the second step, the 0.364% weight loss could be associated with the decomposition of collagen, which starts at 200 °C and continues up to 300 °C (DTA dip at 370.22 °C). The weight loss at around 1.283% (0.517+0.566+0.2) in the temperature ranges of 300 and 450, with a dip at 407, was due to decomposition of organic residues. Since the  $CO_3^{2-}$

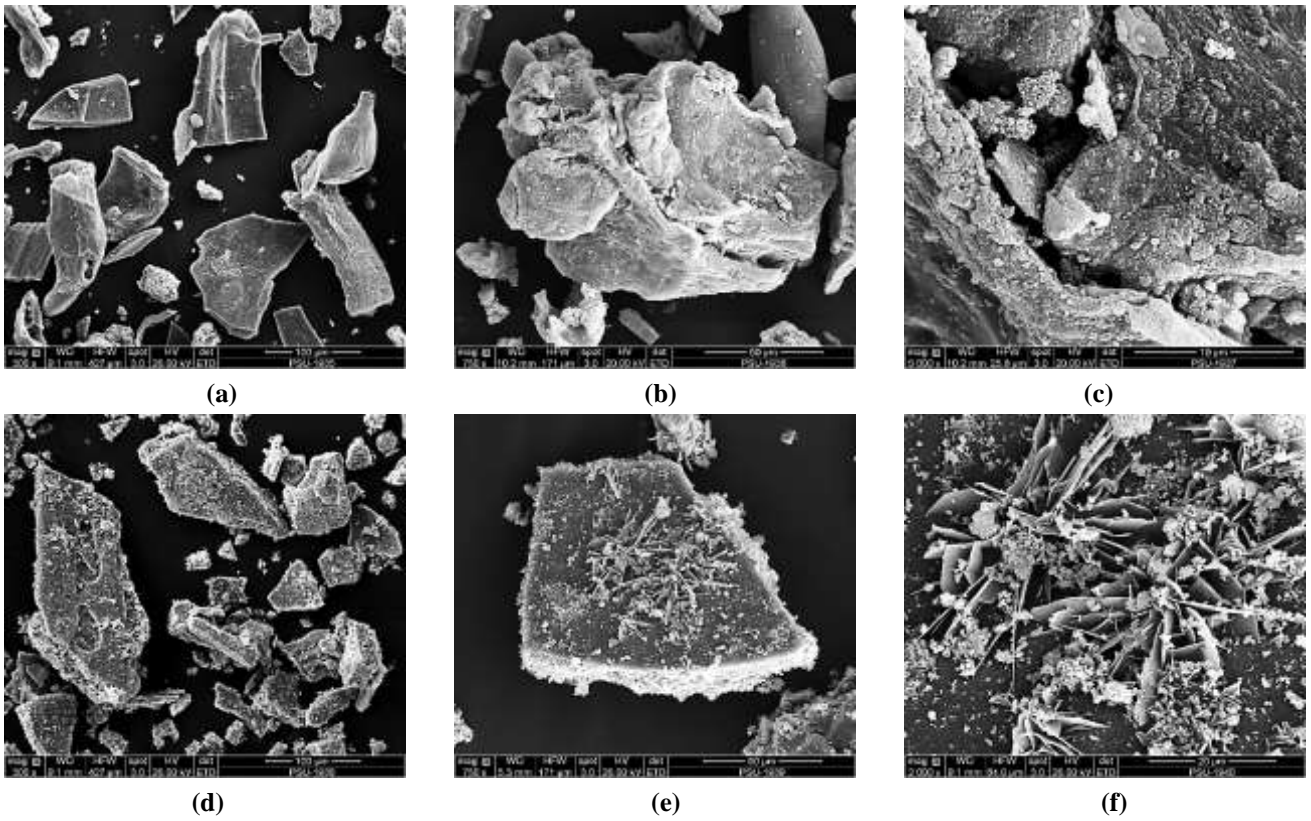


Fig. 3: SEM micrograph of BW sample calcined at 300 °C (a-c) and 600 °C (d-f).

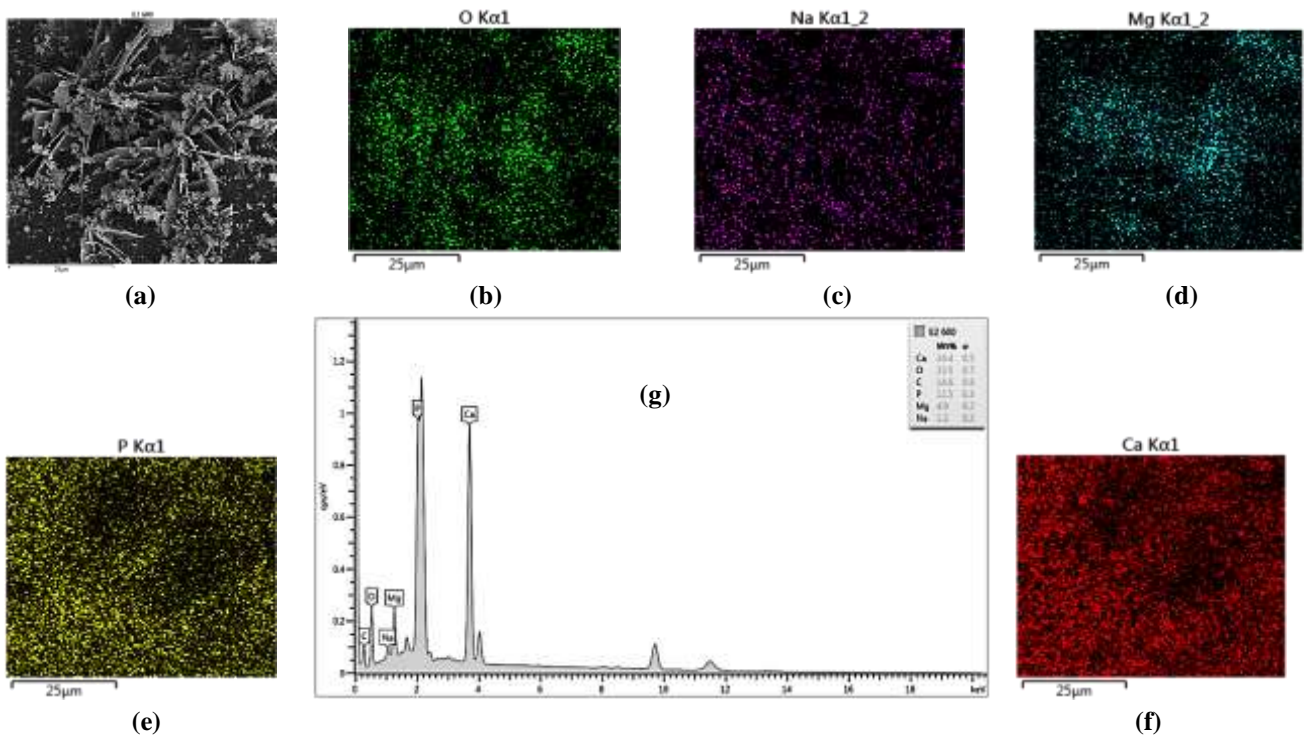


Fig. 4: EDX mapping distribution of oxygen (b), sodium (c), magnesium (d), phosphorous (e), and calcium atoms (f) (a-f) and the EDX spectrum (g) of sample calcined at 600 °C.

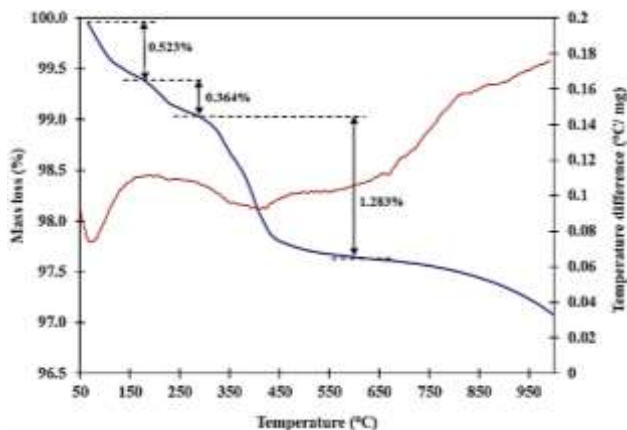


Fig. 5: TGA-DTA curves for sample calcined at 600 °C.

transformation into  $\text{CO}_2$  was taken place at the temperature around 500-600 [31], the slight decrement of 0.688% from 600 to 1000 °C in the TGA curve was assigned to the conversion of HAp to merrillite through hydroxylation reaction [32, 33]. From literature, the merrillite have been converted into others phosphate form such as  $\text{Ca}_3(\text{PO}_4)_2$  with high stabilities up to 1400 °C [34, 35].

#### Fourier transform infrared spectroscopy

FT-IR was performed to identify the functional groups in the synthesized HAp. Fig. 6 depicts the FT-IR spectrum of fresh Budu waste (BW), commercial HAp from Sigma (Com HAP), and various calcined budu waste. For the uncalcined fresh budu, the peaks at 2927  $\text{cm}^{-1}$  and 2853  $\text{cm}^{-1}$  correspond to vibrations of CH groups, while the peaks at 1516  $\text{cm}^{-1}$ , 1410  $\text{cm}^{-1}$ , and 1240  $\text{cm}^{-1}$  corresponded to amide I and amide II bands. The peak related to the carbonyl group appeared at 1590  $\text{cm}^{-1}$ . These peaks were due to the organic compounds in the budu waste [36] and were absent in the powders calcined at temperatures higher than 600 °C. The  $\text{CO}_3^{2-}$ , amide I, and amide II peak intensities decreased with increasing calcination temperature, suggesting a removal of the organic matter. All peaks in the calcined fish bone samples were in agreement with those in the HAp spectra. The most intense peak in the spectra of the samples calcined at 300 °C, 400 °C, and 500 °C was a broad absorption band around 3000 to 3600  $\text{cm}^{-1}$ , which corresponded to the stretching of hydrogen-bonded  $\text{H}_2\text{O}$  molecules [37]. The peaks corresponding to the hydroxyl groups in the HAp crystal at 3570  $\text{cm}^{-1}$  and 631  $\text{cm}^{-1}$  [38] were obtained in the FT-IR spectra of the samples calcined at 600 °C, 700 °C, and 800 °C. The strong band at 961-1093  $\text{cm}^{-1}$  indicated the

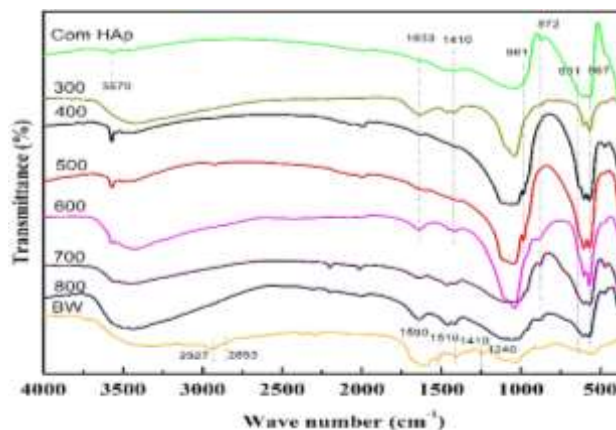


Fig. 6: FT-IR spectra of commercial HAp, untreated BW, and BW calcined at different temperatures.

bending mode of O-P-O [39]. Moreover, the band at 981-983  $\text{cm}^{-1}$  was attributed from the presence of  $\text{PO}_4^{3-}$  ions in the non-apatite/non-stoichiometric environment in merrillite [40]. A band at 567-602  $\text{cm}^{-1}$  corresponded to the symmetric P-O stretching vibration of a  $\text{PO}_4^{3-}$  group. The band at 872  $\text{cm}^{-1}$  corresponded to a presence of  $\text{CO}_3^{2-}$  in the HAp crystal for the sample calcined at 600 °C. Peaks located at 1633  $\text{cm}^{-1}$  and 1410  $\text{cm}^{-1}$  were assigned to the vibrational frequencies of carbonate group in sample.

#### CONCLUSIONS

The HAp was successful synthesized by calcination of Budu waste. Low crystallinity of HAp was obtained when the calcination temperature was lower than 600 °C. The crystallinity of HAp was increased with the increment of calcination temperature. However, the merrillite phase was found when the calcination temperature was higher than 600 °C. This phase can occur by the rearrangement and displacement of  $\text{Mg}^{2+}$  and  $\text{Na}^+$  in the presence of defect and vacancies of  $\text{Ca}^{2+}$  sites. The secondary phase of merrillite presence in the structure was represented by a flower-like shape that able to partly functionalized in such applications. The shapes were regulated the surface structure of inorganic active sites such as the corners, edges, and steps. The sample's crystallinity, sizes, and lattice parameters were identically related to that commercial HAp. As expected, the higher temperatures have led to increase the purities of HAp by incrementing the degrees of crystallinity and crystal sizes. The results finally concluded that the eco-HAp could be prepared from Budu waste by means of the calcination process. The Budu waste will play an important role as a good area

resources provider to synthesise eco-HAP for next future applications. Suggesting a good alternative area with both synthetically and applications in the future.

### Acknowledgment

We would like to thank the Budu Yiseng Factory for providing Budu waste materials, and Yala Rajabhat University, Thailand, for FT-IR equipment support. Our appreciation is also extended to the SC English proofreading service for assistance with the English corrections.

Received: Oct. 9, 2021 ; Accepted: Feb. 28, 2022

### References

- [1] Dorozhkin S.V., [Bioceramics of Calcium Orthophosphates](#), *Biomaterials*, **31(7)**: 1465–1485 (2010).
- [2] Dimović S., Smiciklas I., Plečas I., Antonović D., Mitrić M., [Comparative Study of Differently Treated Animal Bones For Co<sup>2+</sup> Removal](#), *J. Hazard. Mater.*, **164(1)**: 279–87 (2009).
- [3] Pal A., Paul S., Choudhury A.R., Balla V.K., Das M., Sinha A., [Synthesis of Hydroxyapatite from Lates Calcarifer Fish Bone for Biomedical Applications](#), *Mater. Lett.*, **203**: 89–92 (2017).
- [4] Ferraro V., Carvalho A.P., Piccirillo C., Santos M.M., Castro P.M.L., Pintado M.E., [Extraction of High Added Value Biological Compounds from Sardine, Sardine-Type Fish and Mackerel Canning Residues — A Review](#), *Mater. Sci. Eng. C*, **33(6)**: 3111–3120 (2013).
- [5] Cui H., Yang X., Qin J., Tang H., Liu H., Li Y., [Hydrothermal Synthesis and Characterisation of Glutamine-Modified Rod-Like Hydroxyapatite Nanoparticles](#), *Micro. Nano Lett.*, **7(12)**: 1292–1295 (2012).
- [6] Akram M., Ahmed R., Shakir I., Ibrahim W.A.W., Hussain R., [Extracting Hydroxyapatite and Its Precursors From Natural Resources](#), *J. Mater. Sci.*, **49**: 1461–1475 (2014).
- [7] Ozawa M., Suzuki S., [Microstructural Development of Natural Hydroxyapatite Originated from Fishbone Waste Through Heat Treatment](#), *J. Am. Ceram. Soc.*, **85(5)**: 1315–1317 (2002).
- [8] Coelho T.M., Nogueira E.S., Weinand W.R., Lima W.M., Steimacher A., Medina A.N., Baesso M.L., Bento A.C., [Thermal Properties of Natural Nanostructured Hydroxyapatite Extracted from Fish Bone Waste](#), *J. Appl. Phys.*, **101(8)**: 84701 (2007).
- [9] Boutinguiza M., Pou J., Lusquiños F., Comesaña R., Riveiro A., [Production of Calcium Phosphate Nanoparticles By Laser Ablation In Liquid](#), *Phys. Procedia*, **12**: 54–59 (2011).
- [10] Lamkhao S., Phaya M., Jansakun C., Chandet N., Thongkorn K., Rujjanagul G., Bangrak P., Ransom C., [Synthesis of Hydroxyapatite with Antibacterial Properties Using a Microwave-Assisted Combustion Method](#), *Sci. Rep.*, **9**: 4015 (2019).
- [11] Buitrago-Vásquez M., Ossa-Orozco C.P., [Hydrothermal Synthesis of Hydroxyapatite Nanorods Using A Fruit Extract Template](#), *DYNA*, **85(204)**: 283–288 (2018).
- [12] Sánchez-Hernández A.K., Martínez-Juárez J., Gervacio-Arciniega J.J., Silva-González R., Robles-Águila M.J., [Effect of Ultrasound Irradiation on the Synthesis of Hydroxyapatite/Titanium Oxide Nanocomposites](#), *Crystals*, **10(11)**: 1-13 (2020).
- [13] Xiaojun G., Dai L., [Synthesis of Hydroxyapatite Containing Some Trace Amounts Elements in Simulated Body Fluids](#), *Iran. J. Chem. Chem. Eng. (IJCCE)*, **38(1)**: 83-91 (2019).
- [14] Khosravinia S., Kiasat A.Z., [Synthesis and Characterization of  \$\gamma\$ -Fe<sub>2</sub>O<sub>3</sub>@HAp@ \$\beta\$ -CD Core-shell Nanoparticles as a Novel Magnetic Nanoreactor and Its Application in the One-pot Preparation of  \$\beta\$ -azido alcohols,  \$\beta\$ -nitro alcohols, and  \$\beta\$ -cyanohydrins](#), *Iran. J. Chem. Chem. Eng. (IJCCE)*, **38(3)**: 61-68 (2019).
- [15] Mustafa N., Ibrahim M.H.I, Asmawi R., Amin A.M., [Hydroxyapatite Extracted from Waste Fish Bones and Scales via Calcination Method](#), *Appl. Mech. Mater.*, **773–774**: 287–290 (2015).
- [16] Ratna Sunil B., Jagannatham M., [Producing Hydroxyapatite from Fish Bones by Heat Treatment](#), *Mater. Lett.*, **185**: 411-414 (2016).
- [17] Senthil R., Vedakumari S.W., Sastry T.P., [Hydroxyapatite and Demineralized Bone Matrix from Marine Food Waste – A Possible Bone Implant](#), *Am. J. Mater. Synth. Process.*, **3(1)**: 1-6 (2018).



- [18] Permatasari H.A., Wati R., Anggraini R.M., Almukarramah A., Yusuf Y., [Hydroxyapatite Extracted from Fish Bone Wastes by Heat Treatment](#), *Key Eng. Mater.*, **840**: 318–323 (2020).
- [19] Latif A.F.A., Mohd Pu'ad N.A.S., Ramli N.A.A., Muhamad M.S., Abdullah H.Z., Idris M.I., Lee T.C., [Extraction of Biological Hydroxyapatite from Tuna Fish Bone for Biomedical Applications](#), *Mater. Sci. Forum*, **1010**: 584–589 (2020).
- [20] Lolo J.A., Ambali D.P.P., Jefriyanto W., Handayani D., Afridah W., Wikurendra E.A., Amalia R., Syafiuddin A., [Synthesis and Characterization of Hydroxyapatite Derived from Milkfish Bone by Simple Heat Treatments](#), *Biointerface Res. Appl. Chem.*, **12(2)**: 2440 – 2449 (2022)
- [21] Balamurugan A., Rebelo A.H., Lemos A.F., Rocha J.H., Ventura J.M., Ferreira J.M., [Suitability Evaluation Of Sol-Gel Derived Si-substituted Hydroxyapatite for Dental and Maxillofacial Applications Through in Vitro Osteoblasts Response](#), *Dent mater.*, **24(10)**: 1374–1380 (2008).
- [22] Kumar G.S., Rajendran S., Karthi S., Govindan R., Girija E. K., Karunakaran G., Kuznetsov D., [Green Synthesis and Antibacterial Activity of Hydroxyapatite Nanorods for Orthopedic Applications](#), *MRS Comm.*, **7**: 183–188 (2017).
- [23] Mostafa N.Y., [Characterization, Thermal Stability and Sintering of Hydroxyapatite Powders Prepared by Different Routes](#), *Mater Chem. Phys.*, **94(2–3)**: 333-341 (2005).
- [24] Pal A., Paul S., Choudhury A.R., Balla V.K., Das M., Sinha A., [Synthesis of Hydroxyapatite from Lates Calcarifer Fish Bone for Biomedical Applications](#), *Mater. Lett.*, **203**: 89-92 (2017).
- [25] Fu J., He C., Xia B., Li Y., Feng Q., Yin Q., Shi X., Feng X., Wang H., Yao H., [C-axis Preferential Orientation of Hydroxyapatite Accounts for the High Wear Resistance of The Teeth of Black Carp \(\*Mylopharyn godonpiceus\*\)](#), *Sci. Rep.*, **6**: 23509 (2016).
- [26] Rincón-López J.A., Hermann-Muñoz J.A., Giraldo-Betancur A.L., De Vizcaya-Ruiz A., Alvarado-Orozco J.M., Muñoz-Saldaña J., [Synthesis, Characterization and In Vitro Study of Synthetic and Bovine-Derived Hydroxyapatite Ceramics: A Comparison](#), *Materials (Basel)*, **11(3)**: 333 (2018).
- [27] Bigi A., Ripamonti A., [Structure Refinements of Lead-Substituted Calcium Hydroxyapatite by X-ray Powder Fitting](#), *Acta Cryst.*, **45(3)**: 247-251 (1989).
- [28] Lee K.Y., Han Y.C., Suh D.J., Park T.J., [Pb-substituted Hydroxyapatite Catalysts Prepared by Coprecipitation Method for Oxidative Coupling of Methane](#), *Stud. Surf. Sci. Cat.*, **119**: 385-390 (1998).
- [29] John M.H., Bradley L.J., John R., [The Crystal Chemistry of Whitlockite and Merrillite and The Dehydrogenation of Whitlockite to Merrillite](#). *Am. Mineral.*, **93(8-9)**: 1300–1305 (2008).
- [30] Mohd Pu'ad N.A.S., Koshy P., Abdullah H.Z., Idris M.I., Lee T.C., [Syntheses of Hydroxyapatite from Natural Sources](#), *Heliyon*, **5(5)**: e01588 (2019).
- [31] Petkova V., Yaneva V., [Thermal Behavior and Phase Transformations of Nanosized Carbonate Apatite \(Syria\)](#), *J. Therm. Anal. Calorim.*, **99**: 179–189 (2010).
- [32] Shavandi A., Bekhit A. El-Din A., Ali. A., Sun Z., [Synthesis of Nano-Hydroxyapatite \(Nha\) from Waste Mussel Shells Using A Rapid Microwave Method](#), *Mater. Chem. Phys.*, **149–150**: 607-616 (2015).
- [33] Meejoo S., Maneeprakorn W., Winotai P., [Phase and Thermal Stability of Nanocrystalline Hydroxyapatite Prepared via Microwave Heating](#), *Thermochimi. Acta*, **447(1)**: 115-120 (2006).
- [34] Salma-Ancane K., Stipnice L., Borodajenko N., Jakovlevs D., Berzina-Cimdina L., [Incorporation of Magnesium Ions into Synthetic Hydroxyapatite: Synthesis and Characterization](#). *Key Eng. Mater.*, **527**: 26–31 (2012).
- [35] Cacciotti I., Bianco A., Lombardi M., Montanaro L., [Mg-substituted Hydroxyapatite Nanopowders: Synthesis, Thermal Stability and Sintering Behaviour](#), *J. Eur. Ceram. Soc.*, **29(14)**: 2969-2978 (2009).
- [36] C.Y. Ooi, M. Hamdi, S. Ramesh, [Properties of Hydroxyapatite Produced by Annealing of Bovine Bone](#), *Ceram. Int.*, **33(7)**: 1171-1177 (2007).
- [37] Samira M.S., Khairi M.T., Abdelsattar M.S., Lotfi I.A.S., Faten A.M., [Synthesis and Characterization of Hydroxyapatite Contain Chromium](#), *Biophys. Chem.*, **3(4)**: 278-282 (2012).
- [38] Goto T., Sasaki K., [Effects of Trace Elements in Fish Bones on Crystal Characteristics of Hydroxyapatite Obtained by Calcination](#), *Ceram.*, **40(7) Part B**: 10777-10785 (2014).

- [39] Sobczak-Kupiec A., Olender E., Malina D., Tyliczszak B., [Effect of Calcination Parameters on Behavior of Bone Hydroxyapatite in Artificial Saliva and Its Biosafety](#), *Mater. Chem. Phys.*, **206**: 158-165 (2018).
- [40] Ou- Yang H., Paschalis E.P., Boskey A.L., Mendelsohn R., [Two- Dimensional Vibrational Correlation Spectroscopy of In Vitro Hydroxyapatite Maturation](#), *Biopolymers*, **57(3)**:129–139 (2000).